Topological transition in a two-dimensional three-vector model: A non-Boltzmann Monte Carlo study

B. Kamala Latha [1,*] and V. S. S. Sastry[2]

[1]*School of Physics, University of Hyderabad, Hyderabad 500046, India*
[2]*Centre for Modelling, Simulation and Design, University of Hyderabad, Hyderabad 500046, India*

Two-dimensional three-vector ($d = 2$, $n = 3$) lattice model of a liquid crystal (LC) system with order parameter space ($\mathcal{R}$) described by the fundamental group $\Pi_1(\mathcal{R}) = Z_2$ was recently investigated based on non-Boltzmann Monte Carlo simulations. Its results indicated that the system did not undergo a topological transition condensing to a low temperature critical state as was reported earlier. Instead, a crossover to a nematic phase was observed, induced by the onset of a competing relevant length scale. This mechanism is further probed here by assigning a more restrictive $\mathcal{R}$ symmetry with $\Pi_1(\mathcal{R}) = \mathbb{Q}$ (the discrete and non-Abelian group of quaternions), thus engaging the three spin degrees in the formation of point topological defects (disclinations). The results reported here indicate that such a choice of symmetry of the Hamiltonian with suitable model parameters leads to a defect-mediated transition to a low-temperature phase with topological order. It is characterized by a line of critical points with quasi-long-range order of its three spin degrees. The associated temperature-dependent power-law exponent decreases progressively and vanishes linearly as temperature tends to zero. The high-temperature disordered phase shows exponential spin correlations and their temperature-dependent lengths exhibit an essential singular divergence as the system approaches the topological transition point. Biaxial LC models have the required $\mathcal{R}$ symmetry owing to their tensor orientational orders and are suggested to serve as prototype examples to exhibit topological transition in ($d = 2$, $n = 3$) lattice models.

In two-dimensional (2D) lattice systems with three-dimensional spin degrees, ($d = 2$, $n = 3$) models, symmetry of the Hamiltonian H impacts its order parameter space ($\mathcal{R}$) topology [1], determining its first fundamental group $\Pi_1(\mathcal{R})$. In the case of systems with global inversion symmetry of H, $\mathcal{R}$ is isomorphic to RP^2 (three-dimensional real projective space) with fundamental group $\Pi_1(\mathcal{R}) = Z_2$. It hosts an apolar and axially symmetric (uniaxial) order, leading to stable point defects (disclinations). However, this $n = 3$ model could not successfully trigger a defect-mediated Berezenskii-Kosterlitz-Thouless-type (BKT) topological transition [2,3] despite stable topological defects, both in magnetic systems with this order parameter symmetry [4–7] and in liquid crystals [8–14]. A recent Monte Carlo (MC) study based on the density of states (rather than the Metropolis algorithm) [15], indicated the presence of a crossover to a nematic phase. It pointed at the role of the extra spin degree, relative to ($d = 2$, $n = 2$) case, in inducing an additional relevant length scale interfering in the progression from the disordered phase towards the expected topological transition. We probe this system by attempting to suppress the intervening perturbation through a suitable choice of the Hamiltonian symmetry. We facilitate simultaneous participation of all spin degrees in the defect-mediated transition mechanism through an appropriate assignment of the model parameters.

We assign D_2 symmetry to the lattice sites and augment the Lebwohl-Lasher (LL) Hamiltonian [16] (representing an at-

tractive nearest-neighbor biquadratic interaction among, say, molecular z axes) with similar terms among the molecular x axes and y axes. Its $\mathcal{R}$ is represented by the space of cosets $SU(2)/\mathbb{Q}$, where $SU(2)$ is the special unitary group of 2×2 matrices and $\mathbb{Q}$ is the discrete non-Abelian group of quaternions. In this case, $\Pi_1(\mathcal{R}) = \mathbb{Q}$, represented by $(\pm \mathbf{1}, \pm i\sigma_x, \pm i\sigma_y, \pm i\sigma_z)$; $\{\sigma_i\}$ is the set of Pauli matrices. The higher order groups are not relevant to 2D models. The medium hosts four types of stable topological defect structures: three distinct disclinations corresponding to the order directors associated with the three molecular axes (charge 1/2), and equivalent topological defects of unit charge formed by each of the axes. In 2D models, the role of the non-Abelian character of the fundamental group is to make the charge 1/2 defects homotopically inequivalent. The schematics of the defect structures of the three directors are identical to the known counterparts of the single director in the uniaxial nematic medium [1].

We define two orthogonal (uniaxial and biaxial) molecular tensors $\mathbf{q}$ and $\mathbf{b}$, respectively, as $\mathbf{q} := \mathbf{m} \otimes \mathbf{m} - \frac{\mathbf{I}}{3}$ and $\mathbf{b} := \mathbf{e} \otimes \mathbf{e} - \mathbf{e}_\perp \otimes \mathbf{e}_\perp$ where $(\mathbf{e}, \mathbf{e}_\perp, \mathbf{m})$ is an orthonormal set of vectors representing the molecular axes (in the notation of Ref. [17]). The general biquadratic attractive interaction between two lattice sites is given by $H = -U[\xi \, \mathbf{q} \cdot \mathbf{q}' + \gamma(\mathbf{q} \cdot \mathbf{b}' + \mathbf{q}' \cdot \mathbf{b}) + \lambda \mathbf{b} \cdot \mathbf{b}']$. This Hamiltonian, setting $\xi = 1$, was extensively examined in three-dimensional systems in the parameter space of (γ, λ) to elucidate its phase diagram [17–20]. The interaction associated with ξ is conventionally considered dominant determining the degree of ordering of the primary director and is associated with the molecular z axis. In this

*Corresponding author: kklata@gmail.com

Rapid Communication, we set $\gamma = 0$ to avoid cross-coupling interactions without loss of generality. H can be expressed in terms of inner products of the molecular axes (e, $e_\perp$, m), indexing them as (1–3) for convenience. The pairwise interaction between two lattice sites (α, β), then simplifies to $H_{\alpha\beta} = -U\{\xi \ G_{33} + \lambda \ [2(G_{11} + G_{22}) - G_{33}]\}$ (with $\gamma = 0$). Here, $G_{ij} = P_2(f_{ij})$, $P_2(\cdot)$ denotes the second Legendre polynomial, and $f_{ij} = (u_i, v_j)$ is the inner product. The sets of vectors (u_i, $i = 1$–3) and (v_j, $j = 1$–3) are the two triads of molecular axes on the sites (α, β), respectively [21]. Reduced temperature (T) is defined in units of U. With the specific choice of model parameters $\xi = 1$, $\lambda = \frac{1}{3}$, and $\gamma = 0$, H exhibits cyclic permutation symmetry with respect to the indices of the local directors, imparting equally attractive interaction among the three axes. Also, the topological nonequivalence of the three distinct charge 1/2 defects makes the nature and extent of their participation in the respective defect interactions identical and independent. Thus, the description of the well studied transition mechanism based on the energy-entropy arguments in the case of a single type of defects (for example, uniaxial LC system [8,9]) apply equally and separately to the three classes of defects in this model.

The MC simulations are carried out updating single *spin* flips using the Barker-Watts algorithm (random choice of molecular axis followed by random reorientation) [22]. We sample the microstates based on the Wang-Landau algorithm [19,20,23,24], leading to the computation of the density of states (DoS) of the system. An entropic ensemble is then generated (which is distributed uniformly with energy) by effecting the system to perform a random walk in the configuration space guided by the inverse of the DoS. We extract equilibrium ensembles at the desired temperature by assigning two competing probability weight factors to each member of the entropic ensemble. The density of states favors high energy states, whereas the temperature-dependent Boltzmann factor prefers lower energy. The microstates of the entropic ensemble are accepted, or otherwise, as per the resulting probability, leading to an equilibrium distribution of microstates appropriate to the chosen temperature, known as the reweighting procedure. Equilibrium values of different physical properties of interest are averaged over these generated equilibrium ensembles (typically comprising $\gtrsim 10^6$ microstates) at 10^3 temperatures covering the range [0.05–1.5]. We consider interactions of the nearest-neighbor sites on 2D square lattices with different sizes $L \times L$ ($L = 60, 80, 100, 120, 150$) and apply periodic boundary conditions. The equilibrium properties computed include ensemble averages of the system energy per site $E = \langle E_c \rangle / L^2$ (E_c is the configuration energy of the microstate), the specific heat per site $C_v = (\langle E_c^2 \rangle - \langle E_c \rangle^2)/L^2 T^2$, the uniaxial orientational order R_{00}^2 and biaxial order R_{22}^2 along with their susceptibilities, $\chi_{00}^2 [= (L^2 \langle (R_{00}^2)^2 \rangle - \langle R_{00}^2 \rangle^2)/T]$ and $\chi_{22}^2 [= (L^2 \langle (R_{22}^2)^2 \rangle - \langle R_{22}^2 \rangle^2)/T]$. The macroscopic orientational order parameters (R_{00}^2 and R_{22}^2) are identified with the two dominant weight factors in the expansion of the mean-field tensors in terms of the mutually orthogonal basis tensors (of uniaxial and biaxial symmetry) in the laboratory frame [25,26].

In addition, we also computed the topological parameters of the dominant charge 1/2 defects of the three order directors.

The fourth permissible charge 1 defect was not observable due to its extremely low probability of occurrence arising from energetic reasons [11,27]. The topological order parameter μ_z, of say, the z-axis director forming the charge 1/2 defect, is calculated as proposed earlier [8] and elaborated in Ref. [11]. We assign a unit vector $s(r)$ at each site r on the square lattice representing the local z-director orientation. We consider a three-dimensional unit sphere with the antipodal points identified to define the RP^2 space of the director associated with the molecular z axis. The position of each of the lattice vectors is a point on this surface. Considering z-vector values at two neighboring lattice sites, (r, r'), we assign a path on the surface of this sphere in $\mathcal{R}$ by choosing the shortest geodesic connecting them. Any closed loop on the lattice $\mathcal{L}$ is thus mapped to a loop in the order parameter space of the associated axis (z axis in this case). The homotopy class of this map is given by $\mathcal{W}(\mathcal{L}) = \prod_{(r, r') \in \mathcal{L}} \text{sgn}[s(r), s(r')]$ where the product is sequentially ordered over $\mathcal{L}$ and sgn operates on the inner product of the two vectors. Topological order μ_z is computed as the ensemble average of $\mathcal{W}(\mathcal{L})$ on a closed loop generated by the toroid over the lattice (making use of periodic boundary conditions). It is useful to calculate a related parameter δ_z defined by $\delta_z = (1 - \mu_z)/2$ [8]. We computed the density of unbounded charge 1/2 defects d_z of the director associated with the z axis by dividing the lattice into a composition of elementary triangular plaquettes. The above product applied to each plaquette yields a defect finding algorithm: If the ordered product is -1, the plaquette encloses a charge 1/2 defect. The average defect density d_z is calculated from the total count of such isolated defects over the lattice and averaged over the ensemble [11]. The topological parameters of the other two directors (δ_x, δ_y; d_x, d_y) are similarly computed. Pair correlation functions of the spatial variation of reorientational fluctuations $G(r_{ij}) = \langle P_2 (r_i, r_j) \rangle$ are computed for the three directors (at $L = 150$) at about 80 temperatures. Statistical errors, estimated with the jack-knife algorithm [28], in E, R_{00}^2, R_{22}^2, $\delta_{(x,y,z)}$, and $d_{x,y,z}$ are typically of the order of 1 in 10^3, whereas higher moments (C_v, χ_{00}^2, χ_{22}^2) are relatively less accurate (about 5 in 10^2).

Figure 1 depicts the temperature variation of C_v which is independent of the system size, unlike in a normal order-disorder transition, and is consistent with earlier observations [29]. At these system sizes, the energy E is found to be size independent [see inset (a)]. Due to the permutation symmetry of the system, the topological defect densities associated with different directors as well as the corresponding topological orders are insensitive to their index, and so we present the data on the z-axis director, representative of the other two axes as well. Inset (b) shows the temperature variation of d_z which is found to be size independent, but for very marginal size dependence at the onset of the transition on the low-temperature side ($T \sim 0.7$). The profile of the temperature derivative of the defect density is qualitatively similar to that of the specific heat, hinting at the mechanism for the onset of the observed size-independent cusp of the specific heat [8,30].

Figure 2 shows the size dependence of R_{00}^2 and R_{22}^2, plotted as a function of temperature. At the onset temperature, their size dependence is curiously different from the regular transitions; the degree of order decreases with increasing L notably
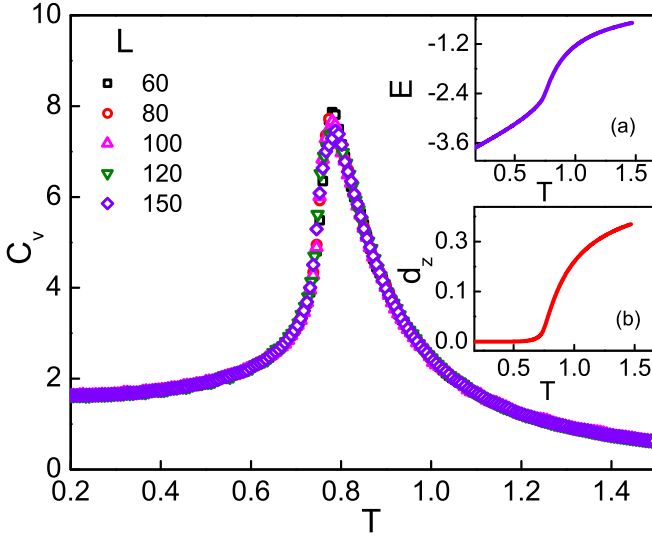
FIG. 1. Temperature variation of specific heat (per site) at lattice sizes $L = 60, 80, 100, 120,$ and 150. Insets show the temperature variation of (a) size independent energy per site, and (b) topological density at $L = 150$.

FIG. 3. Temperature variation of topological parameter δ_z at lattice sizes $L = 60, 80, 100, 120,$ and 150. Inset (a) shows inflexion point of δ_z at $L = 80$ (dashed vertical line) indicating the unbinding transition temperature $T_{U\delta}$; (b) finite-size scaling plot of $T_{U\delta}(L)$.

at the onset of the transition (characteristic of a topological transition [10,14]) and converge at very low temperatures (Fig. 2). Inset (a) depicts the temperature variation of the uniaxial susceptibility χ_{00}^2 showing peaks at the respective transition temperatures. Their peak positions shift slightly to lower temperature with L, and their low-temperature profiles indicate progressively enhanced values with size. General features of the orientational order and its susceptibility observed are typical of topological transitions [10,14,29]. The peak values of χ_{00}^2 at different L's, say $\chi_0(L)$, are noted for further analysis.
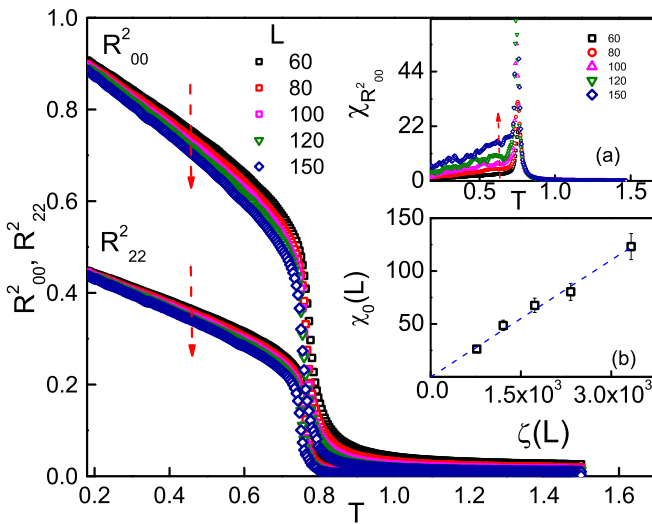

FIG. 2. Temperature variation of orientational order parameters at lattice sizes $L = 60, 80, 100, 120,$ and 150. Insets show the temperature variation of (a) uniaxial susceptibility, (b) finite-size scaling plot of the peak value of susceptibility $\chi_0(L)$. The dashed arrows are indicative of the variation of the parameter with an increase in system size.
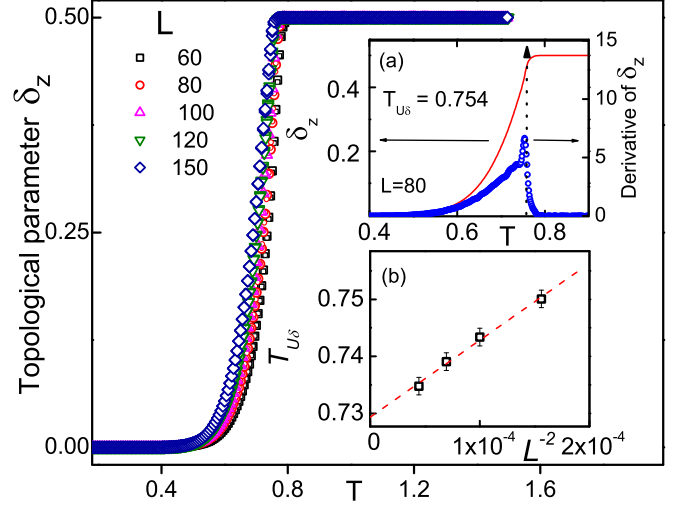
Figure 3 depicts the size dependence of the temperature profiles of δ_z showing a gradual shift to lower temperatures with increase in size–much like the orientational order profiles and their susceptibility peak positions (see Fig. 2). The inflexion point of the topological order parameter δ_z with respect to T corresponds to the unbinding transition temperature at that system size $T_{U\delta}(L)$. The inset (a) of Fig. 3 depicts its temperature derivative at $L = 80$ with a peak at $T_{U\delta}(L) = 0.754 \ (\pm 0.002)$. Inset (b) of Fig. 3 is a finite-size scaling (FSS) plot of such transition temperatures derived from topological parameter profiles at different sizes. The results lead to a reasonable fit, yielding an estimate of the unbinding temperature derived from this parameter as $T_{U\delta} = 0.727 \ (\pm 0.002)$ in the thermodynamic limit.

Spatial variations of $G(r)$ at $L = 150$, (depicting only a subset of the data collected at about 80 temperatures), are shown in Fig. 4, each profile representing identical variation of the three directors at that temperature. For $T \lesssim 0.73$, the correlation functions obey power-law decays very well $G(r, T) \approx r^{-\eta(T)}$, yielding a temperature-dependent exponent $\eta(T)$ (within 1% error). Figure 5 shows the variation of $\eta(T)$ in the low-temperature region leading up to to the transition temperature (graph corresponding to the left abscissa). $\eta(T)$ is found to decrease with lowering the temperature, and it vanishes linearly as $T \rightarrow 0$. We note that its temperature variation near the transition, $T \approx T_{U\delta}$ appears to fit to a power law. Accordingly, we fit the data to the expression $\eta(T) = B(T_{U\eta} - T)^{\kappa} + \eta_{T_U}$ to determine the asymptotic value of the unbinding temperature $T_{U\eta}$ and the corresponding limiting exponent η_{T_U}. We obtain a very satisfactory fit, yielding $T_{U\eta}(L = 150) = 0.729 \pm 0.001$, $\kappa = 0.485 \pm 0.005$, $\eta_{T_U} = 0.342 \pm 0.003$, and $B = 0.399 \pm 0.002$. This value of the index η compares well from the earlier studies on the LL model investigating this transition: 0.325 [10] and 0.338 [14]. This estimate of the unbinding transition temperature derived from the low-temperature correlation function data compares well within errors with the
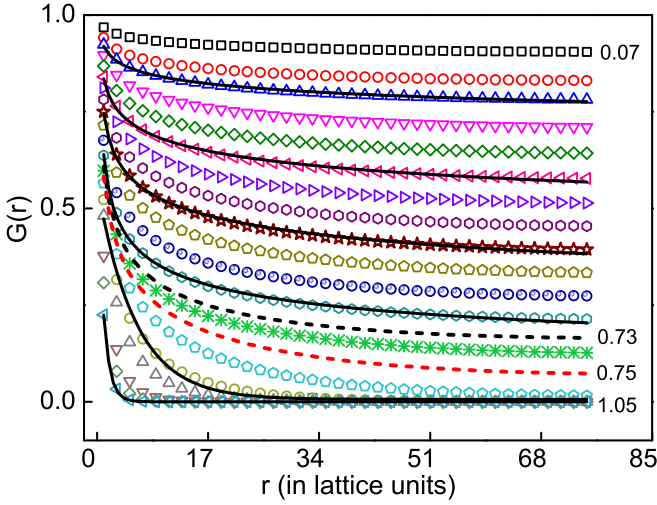
FIG. 4. Spatial variation of correlation functions $G(r)$ at representative temperatures bracketing the transition ($L = 150$). $G(r)$ fits well to exponential decays above $T = 0.75$, whereas it exhibits a power-law variation below $T = 0.73$. These bounding decays are indicated in the figure as dashed lines. The fit curves both above and below the transition temperature are superimposed on the corresponding data points as solid lines at a few representative temperatures ($T = 0.17, 0.35, 0.53, 0.7, 0.78,$ and 1.05).

corresponding $T_{U\delta}$ ($=0.734$, both computed at $L = 150$). The linear temperature variation of $\eta(T)$ (short dashed line from the origin in Fig. 5) and its vanishing as $T \to 0$ are signatures of spin-wave contribution at low temperatures. The increase in the peak values of the susceptibility with size, $\chi_0(L)$ [from inset (a) in Fig. 2], is analyzed based on FSS arguments as [31]
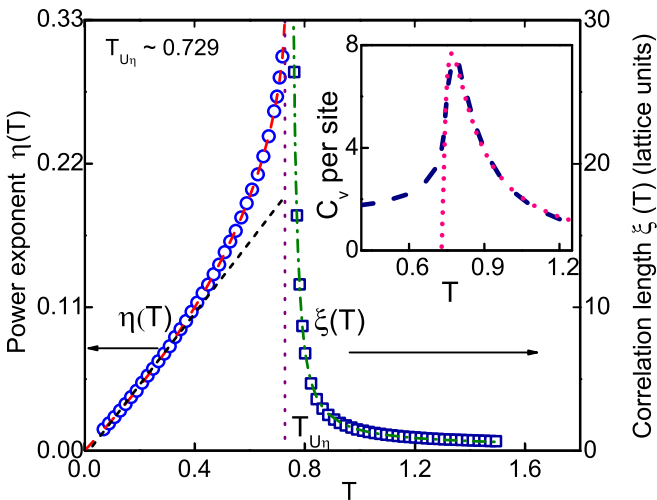

FIG. 5. Temperature variation of the exponent $\eta(T)$ and correlation length $\xi(T)$ at $L = 150$. The curved dashed line (left) is the power-law fit of $\eta(T)$, and the dashed-dotted line (right) is a divergence fit of $\xi(T)$ as indicated in the text. The short dashed straight line from the origin is a linear fit of $\eta(T)$ data at low temperatures. The inset shows the critical contribution to the C_v (short dashes) superposed on the C_v profile (long dashes) depicted over the entire temperature range. The critical contribution vanishes at the transition temperature $T \approx 0.727$.

$\chi_0(L) \sim \zeta(L) = KL^{(2-\eta_{T_U})}(lnL)^{-2r}$ with fit parameters $\eta_{T_U} = 0.342$ (as computed above and held fixed), $r = 0.0625$ (at fixed BKT value), and the nonuniversal fit parameter $K = 0.0368$. The satisfactory fit [inset (b) of Fig. 2] shows the divergence of the susceptibility at the transition point with increasing system size and is in accord with a similar observation on the topological transition assigned to the 2D LL model [10].

The $G(r)$ profiles for $T \geqslant 0.75$ fit very well to decays given by $G(r, T) = Ar^{-\eta_{T_U}} \exp[-r/\xi(T)] + A_0$, facilitating estimation of temperature-dependent system length scale $\xi(T)$ (within 2% error) originating from correlations limited by the unbounded defect density in the disordered state. Here, A is a nonuniversal constant, A_0 is related to long-range orientational order, and η_{T_U} is known from the fit of the low-temperature $G(r)$ data. In the narrow temperature range [0.73–0.75], functional dependence of $G(r)$ could not be assigned satisfactorily to either of the above decay functions, showing relatively much higher least-squares errors, and this region is indicated by two decays in dashed lines in Fig. 4.

The temperature variation of $\xi(T)$ is also shown in Fig. 5 (the graph corresponding to the right abscissa). Its observed sharp increase is fit to the general mean-field expression accounting for its divergence due to the sudden disappearance of unbound defects (Z_2 vortices) near the transition temperature, given by $\xi(T) \approx \exp[\frac{D}{(T-T_{U\eta})^\nu}]$ [3,5,31]. The estimated value of the transition temperature $T_{U\eta}(L = 150) = 0.729$ from the low-temperature $G(r)$ data is used as a fixed parameter in the above expression. This analysis yields the critical index associated with length scale $\xi(T)$ as $\nu = 0.304 \pm 0.004$. With the computed values of $T_{U\eta}$ and ν thus obtained from $G(r)$, the critical contribution to the specific heat above the transition temperature is generated and compared with the data obtained from MC simulation. We note that the system free energy $\Phi \sim \xi^{-2}$, and the critical contribution to the the specific heat C_v (as its temperature derivative [5]), is given by $C_v \approx (\frac{C}{(T-T_{U\eta})})^{2(\nu+1)} \exp[-2(\frac{C}{(T-T_{U\eta})})^\nu]$. The C_v profile of the disordered phase above the transition temperature (Fig. 1) is fit to this expression along with an additive background term to account for noncritical contributions. The fit parameters are nonuniversal constants. The inset of Fig. 5 shows the MC simulated data over the entire temperature region, superimposed by the fit curve to the above expression, accounting for the critical contribution plus the background. It may be noted that the critical contribution vanishes at the unbinding temperature as a weak essential singularity. The cusp of the specific heat peak above this singular point originates from the rapid proliferation of the unbound defects at the onset of the unbinding transition as reflected by the rapid growth of defect density [shown in the inset (b) of Fig. 1]. The critical indices derived from the temperature variation of $G(r)$ account very satisfactorily for the critical contributions to the specific heat of the system, generated with the model of a defect-mediated topological transition. The power-law variation of $G(r, T)$ below the unbinding temperature $T_{U\eta}(\approx T_{U\delta}) = 0.729$ characterizes the quasi-long-range order of the medium in the low-temperature phase representing a line of critical points, considered to be the unique signature of a topologically ordered state.

These results convincingly demonstrate the onset of a BKT-type defect-unbinding transition in the ($d = 2$, $n = 3$) LC model in the presence of topologically distinct classes of disclination (charge 1/2) points of the three spin degrees, aided by their simultaneous participation in the defect kinetics. Biaxial LC models in this context are seen as plausible examples and serve as models to probe this transition. The generalized biquadratic Hamiltonian model with a suitable choice of the parameters so as to lead to a direct transition from the disordered state to a low-temperature phase with biaxial symmetry serves as a prototype 2D model with three spin degrees to condense to a critical low-temperature phase through a topological transition.

[1] N. D. Mermin, Rev. Mod. Phys. **51**, 591 (1979).

[2] V. L. Berezenskii, Zh. Eksp. Teor. Fiz. **59**, 907 (1970) [Sov. Phys. JETP **32**, 493 (1971)]; Zh. Eksp. Teor. Fiz. **61**, 114 (1971) [Sov. Phys. JETP **34**, 610 (1972)].

[3] J. M. Kosterlitz and D. J. Thouless, J. Phys. C **6**, 1181 (1973).

[4] M. Wintel, H. U. Everts, and W. Apel, Phys. Rev. B **52**, 13480 (1995).

[5] H. Kawamura, A. Yamamoto, and T. Okubo, J. Phys. Soc. Jpn. **79**, 023701 (2010).

[6] N. Hasselmann and A. Sinner, Phys. Rev. B **90**, 094404 (2014).

[7] I. S. Popov, P. V. Prudnikov, A. N. Ignatenko, and A. A. Katanin, Phys. Rev. B **95**, 134437 (2017).

[8] H. Kunz and G. Zumbach, Phys. Rev. B **46**, 662 (1992).

[9] B. Berche and R. Paredes, Condens. Matter Phys. **8**, 723 (2005).

[10] E. Mondal and S. K. Roy, Phys. Lett. A **312**, 397 (2003).

[11] S. Dutta and S. K. Roy, Phys. Rev. E **70**, 066125 (2004).

[12] S. Shabnam, S. D. Gupta, and S. K. Roy, Phys. Lett. A **380**, 667 (2016).

[13] R. Paredes V., A. I. Farinas-Sanchez, and R. Botet, Phys. Rev. E **78**, 051706 (2008).

[14] A. I. Farinas-Sanchez, R. Botet, B. Berche, and R. Paredes, Condens. Matter. Phys. **13**, 13601 (2010).

[15] B. K. Latha and V. S. S. Sastry, Phys. Rev. Lett. **121**, 217801 (2018).

[16] P. A. Lebwohl and G. Lasher, Phys. Rev. A **6**, 426 (1973).

[17] A. M. Sonnet, E. G. Virga, and G. E. Durand, Phys. Rev. E **67**, 061701 (2003).

[18] F. Bisi, E. G. Virga, E. C. Gartland, Jr., G. DeMatteis, A. M. Sonnet, and G. E. Durand, Phys. Rev. E **73**, 051709 (2006).

[19] B. Kamala Latha, R. Jose, K. P. N. Murthy, and V. S. S. Sastry, Phys. Rev. E **92**, 012505 (2015).

[20] B. Kamala Latha and V. S. S. Sastry, Liq. Cryst. **45**, 2197 (2018).

[21] S. Romano, Physica A **337**, 505 (2004).

[22] J. A. Barker and R. O. Watts, Chem. Phys. Lett. **3**, 144 (1969).

[23] F. Wang and D. P. Landau, Phys. Rev. Lett. **86**, 2050 (2001); Phys. Rev. E **64**, 056101 (2001).

[24] D. Jayasri, V. S. S. Sastry, and K. P. N. Murthy, Phys. Rev. E **72**, 036702 (2005).

[25] F. Bisi, S. Romano, and E. G. Virga, Phys. Rev. E **75**, 041705 (2007).

[26] R. Berardi, L. Muccioli, S. Orlandi, M. Ricci, and C. Zannoni, J. Phys.: Condens. Matter **20**, 463101 (2008).

[27] M. Hindmarsh, Phys. Rev. Lett. **75**, 2502 (1995).

[28] B. Kamala Latha, G. Sai Preeti, K. P. N. Murthy, and V. S. S. Sastry, Comput. Mater. Sci. **118**, 224 (2016).

[29] A. I. Fariñas-Sánchez, R. Paredes, and B. Berche, Phys. Rev. E **72**, 031711 (2005).

[30] C. Holm and W. Janke, J. Phys. A **27**, 2553 (1994).

[31] R. Kenna, Condens. Matter. Phys. **9**, 283 (2006).